Inorganic Chemistry
ARTICLE
pubs.acs.org/IC

Structural Flexibility and Role of Vicinal 2-Thienyl Rings in 2, 3-Dicyano-5,6-di(2-thienyl)-1,4-pyrazine, $[(CN)_2Th_2Pyz]$, Its Palladium(II) Complex $[(CN)_2Th_2Pyz(PdCl_2)_2]$, and the Related Pentametallic Pyrazinoporphyrazines $[(PdCl_2)_4Th_8TPyzPzM]$ (M = $Mg^{II}(H_2O)$, Zn^{II})

Maria Pia Donzello,[*,†] Giorgia De Mori,[†] Elisa Viola,[†] Claudio Ercolani,[†] Enrico Bodo,[†] Luisa Mannina[‡,§] Donatella Capitani,[§] Corrado Rizzoli,[⊥] Lorenzo Gontrani,[†] Giuliana Aquilanti,[‖] Karl M. Kadish,[⊗] and Paola D'Angelo[†]

[†]Dipartimento di Chimica and [‡]Dipartimento di Chimica e Tecnologie del Farmaco, Università "Sapienza", P.le A. Moro 5, I-00185 Rome, Italy

[§]Laboratorio di Risonanza Magnetica "Annalaura Segre", Istituto di Metodologie Chimiche, CNR, I-00015 Monterotondo, Roma, Italy

[⊥]Dipartimento di Chimica Generale ed Inorganica, Università di Parma, Viale delle Scienze, I-43100 Parma, Italy

[‖]Sincrotrone Trieste S.C.p.A., Strada Statale 14, km 163.5, I-34149 Basovizza, Trieste, Italy

[⊗]Department of Chemistry, University of Houston, Houston, Texas, 77204-5003, United States

Supporting Information

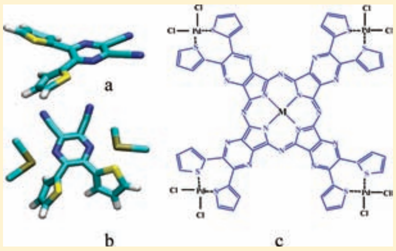

ABSTRACT: The solid state and solution structure of 2,3-dicyano-5,6-di(2-thienyl)-1, 4-pyrazine, $[(CN)_2Th_2Pyz]$, and its Pd^{II} derivative, $[(CN)_2Th_2Pyz(PdCl_2)_2]\cdot H_2O$, formed by reaction of $[(CN)_2Th_2Pyz]$ with $[(C_6H_5CN)_2PdCl_2]$ were characterized by X-ray, UV−visible, ^1H and ^{13}C NMR, and extended X-ray absorption fine structure (EXAFS) spectral measurements. The X-ray crystal structure of $[(CN)_2Th_2Pyz]$ shows the presence of one thienyl ring positioned orthogonal to the rest of the molecule, with the two vicinal thienyl rings lying orthogonal to each other in a rare arrangement. NMR studies of $[(CN)_2Th_2Pyz]$ in the solid state and in solutions of dimethylformamide or dimethyl sulfoxide confirm a nonequivalence of the thienyl rings in the solid state and also in solution. EXAFS results indicate that two distinct Pd^{II} coordination sites are formed at the di(2-thienyl)pyrazino moiety of $[(CN)_2Th_2Pyz(PdCl_2)_2]\cdot H_2O$, with identical Pd−$N_{pyz}$ (2.03(3) Å) and Pd−Cl (2.36(3) Å) bond lengths but with different Pd−S1 (2.25(4) Å) and Pd−S2 (3.21(5) Å) bond distances in an overall asymmetric molecular framework. Density functional theory (DFT) and time-dependent DFT (TDDFT) theoretical studies also provide information about the structure and spectral behavior of the precursor and its metalated Pd^{II} derivative. $^1H/^{13}C$ NMR and UV−visible spectral measurements were also carried out on two heteropentametallic porphyrazine macrocycles which were prepared by a reaction of $PdCl_2$ with $[Th_8TPyzPzM]$ where $Th_8TPyzPz$ = tetrakis-2,3-[5,6-di-(2-thienyl)-pyrazino]porphyrazinato dianion and M = $Mg^{II}(H_2O)$ or Zn^{II}. Spectroscopic data on the newly synthesized $[(PdCl_2)_4Th_8TPyzPzM]$ compounds suggest that the binding of $PdCl_2$ involves coordination sites of the type $S_{2(th)}PdCl_2$ with the two thienyl rings of each di(2-thienyl)pyrazino fragment bound to Pd^{II} in an equivalent manner ("th-th" coordination). This is similar to what was found for the corresponding octapyridinated analogues ("py-py" coordination).

INTRODUCTION

The UV−visible spectral features and redox behavior of 2, 3-dicyano-5,6-di(2-thienyl)-1,4-pyrazine, $[(CN)_2Th_2Pyz]$ (Chart 1A), and its structurally similar dipyridinated analogue, $[(CN)_2Py_2Pyz]$ (Chart 1B), were previously reported.[1] $[(CN)_2Py_2Pyz]$, was also structurally characterized[2a] and forms both monopalladated, $[(CN)_2Py_2PyzPdCl_2]$,[2b] and monoplatinated, $[(CN)_2Py_2PyzPtCl_2]$,[1] derivatives in which the $PdCl_2$ or $PtCl_2$ units are coordinated to the N atoms of the two pyridine rings ("py-py" coordination). $[(CN)_2Py_2Pyz]$ is able to autocyclotetramerize, resulting in formation of the corresponding free-base porphyrazine compound $[Py_8TPyzPzH_2]$,[2a] from which a number of corresponding metalloporphyrazines with the formula $[Py_8TPyzPzM]$ (M = $Mg^{II}(H_2O)$, Mn^{II}, Co^{II}, Cu^{II}, Zn^{II}, Pd^{II}) were prepared and characterized.[2b−d] These porphyrazine compounds could be converted into their corresponding octacations[2b,e,f] and were shown to undergo exocyclic coordination leading to the formation of homo-[2b] and heteropentametallic complexes,[2g] these latter species also containing the external $PdCl_2$ units coordinated in a "py-py" fashion.[2b,g]

Our detailed investigations into the chemistry of $[(CN)_2Py_2Pyz]$ and its related larger macrocycles led us to also consider the bis-thienyl compound $[(CN)_2Th_2Pyz]$ for a parallel study. As recently reported,[3] $[(CN)_2Th_2Pyz]$ is used as a precursor for

Received: August 3, 2011
Published: October 31, 2011

Chart 1. Schematic Representation of (A) [$(CN)_2Th_2Pyz$] and (B) [$(CN)_2Py_2Pyz$]

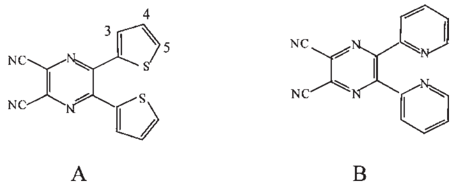

Figure 1. Schematic representation of the macrocycles [$Th_8TPyzPzM$].

the formation of the porphyrazine macrocycles [$Th_8TPyzPzM$] ($Th_8TPyzPz$ = tetrakis-2,3-[5,6-di-(2-thienyl)-pyrazino]porphyrazinato dianion; M = $2H^1$, $Mg^{II}(H_2O)$, Zn^{II}, Co^{II}, Cu^{II}) (Figure 1), following previous work on the Mg^{II} and Zn^{II} compounds.[4]

One interesting feature of the bis-thienyl compound [$(CN)_2Th_2Pyz$] is its binding capacity to metal centers. The coordination ability of the di(2-thienyl)pyrazino fragment is quite intriguing, in part because multiple modes of metal-to-thienyl ring binding are possible (see Supporting Information, Scheme S1), and also because in the di(2-thienyl)pyrazino fragment of [$(CN)_2Th_2Pyz$] there are two 2-thienyl rings in a vicinal position which may further modulate the types of coordination to metal centers.

The target of the present contribution is primarily to establish the type of metal coordination to the di(2-thienyl)pyrazino site of [$(CN)_2Th_2Pyz$] and the related porphyrazine macrocycles, while also clarifying the level of participation to the binding of the N_2S_2 donor set present in both types of compounds. This is a rarely occurring coordination environment for the presence of the 2-thienyl rings in a vicinal position, and represents a problematic aspect to our knowledge not so far addressed in the literature.

Our first goal was to obtain information about the reciprocal positioning of the two 2-thienyl rings relative to each other and also relative to the pyrazine ring in the precursor [$(CN)_2Th_2Pyz$], and to then examine, as a whole, the structural arrangement and flexibility of the di(2-thienyl)pyrazino fragment. To accomplish this, single crystal X-ray work and NMR experiments of the thienyl compound were carried out in the solid state and in solution and are presented in the current paper. The involvement of the thienyl residues of [$(CN)_2Th_2Pyz$] in the Pd^{II} coordination of [$(CN)_2Th_2Pyz(PdCl_2)_2$]$\cdot H_2O$ were studied by NMR and extended X-ray absorption fine structure (EXAFS) measurements and are supported by density functional theory (DFT) and time-dependent DFT (TDDFT) calculations, the latter also being of help with interpretation of the UV–visible spectral features of [$(CN)_2Th_2Pyz$] and its bis-Pd^{II} derivative. To increase our knowledge about the role played by the vicinal groups in metal coordination, the present work also reports the synthesis and physicochemical characterization of two related pentametallic porphyrazine macrocycles which contain $PdCl_2$ units peripherally bound to the di(2-thienyl)pyrazino fragments. These are represented as [$(PdCl_2)_4Th_8TPyzPzM$] where M = $Mg^{II}(H_2O)$ or Zn^{II}.

EXPERIMENTAL SECTION

Solvents and reagents were purchased and used without further purification. The synthesis of [$(CN)_2Th_2Pyz$] from 2,2′-thienyl and diaminomaleonitrile was previously reported,[4a] with further details given recently,[3] including the isolation of yellow orange needle crystals suitable for single crystal X-ray work. The monometallic macrocycles [$Th_8TPyzPzMg(H_2O)$]$\cdot 3H_2O$, [$Th_8TPyzPzZn$]$\cdot 4H_2O$, and [$Th_8TPyzPzH_2$]$\cdot CF_3COOH\cdot H_2O$ were obtained following reported procedures.[3] [$(C_6H_5CN)_2PdCl_2$] was prepared as described elsewhere.[5]

[$(CN)_2Th_2Pyz(PdCl_2)_2$]$\cdot$$H_2O$. [$(CN)_2Th_2Pyz$] (52.0 mg; 0.177 mmol) and [$(C_6H_5CN)_2PdCl_2$] (139.4 mg, 0.363 mmol) (molar ratio: 1/2.05) were added to CH_3OH (15 mL), and the mixture was kept at 80 °C for 1.5 h. After cooling and centrifugation, the solid orange-red material was washed repeatedly with CH_3OH and brought to constant weight under vacuum (10^{-2} mmHg; 52 mg, yield 44%). Calcd for [$(CN)_2Th_2Pyz(PdCl_2)_2$]$\cdot H_2O$, $C_{14}H_8Cl_4N_4OPd_2S_2$: C, 25.21; H, 1.21; N, 8.40; S, 9.61; Pd, 31.91. Found C, 25.82; H, 1.59; N, 9.88; S, 8.98; Pd, 32.07%. IR (cm^{-1}, KBr): 3400 (broad), 1614 (w), 1425 (w), 1380 (s), 875 (vw), 841 (vw), 825 (vw), 723 (w), 350 (ν Pd–Cl, w). Thermogravimetric analysis shows a weight loss of 2.40% (calcd value per one water molecule: 2.79%). The X-ray powder spectrum is indicative of an amorphous material. All attempts to obtain the complex in a crystalline form, suitable for X-ray analysis were unsuccessful. Noteworthy, no tendency toward formation of the monopalladate compound [$(CN)_2Th_2PyzPdCl_2$] was observed, even using appropriate ratios of the reactants [$(CN)_2Th_2Pyz$] and [$(C_6H_5CN)_2PdCl_2$] (~ 1:1).

[$(PdCl_2)_4Th_8TPyzPzMg(H_2O)$]$\cdot$$2H_2O$. [$Th_8TPyzPzMg(H_2O)$]$\cdot 2H_2O$ (54.6 mg, 0.043 mmol) and $PdCl_2$ (48 mg, 27 mmol) (molar ratio 1:6) were suspended in THF (4 mL), and the mixture was kept to reflux under stirring for 65 h. After cooling and centrifugation, the dark-green solid separated was washed repeatedly with water and acetone and brought to constant weight under vacuum (10^{-2} mmHg) (49 mg; yield 58%). Calcd for $C_{56}H_{30}Cl_8MgN_{16}O_3Pd_4S_8$: C, 34.23; H, 1.54; N, 11.40; S, 13.05; Pd, 21.66. Found: C, 34.47; H, 1.82; N, 10.55; S, 12.89; Pd, 20.69%. IR (KBr, cm^{-1}): 3400 (broad), 1627 (w), 1516 (m), 1419 (m-s), 1385 (s), 1362 (m), 1313 (m-s), 1252 (m), 1230 (m), 1176 (m), 1084 (m), 1063 (vw), 1045 (vw), 904 (m-s), 854 (m), 777 (s), 746 (m), 704 (vs), 335 (ν Pd–Cl, w).

[$(PdCl_2)_4Th_8TPyzPzZn$]$\cdot$$6H_2O$. [$Th_8TPyzPzZn$]$\cdot 4H_2O$ (20.5 mg, 0.016 mmol) and $PdCl_2$ (13.5 mg, 0.08 mmol) (molar ratio 1:5) were suspended (partly dissolved) in tetrahydrofuran (THF, 4 mL), and the mixture was heated to reflux under stirring for 75 h. After cooling and centrifugation, the dark-green solid was washed repeatedly with water, twice with acetone, and brought to constant weight under vacuum (10^{-2} mmHg) (15.8 mg; yield 48%). Calcd for $C_{56}H_{36}Cl_8N_{16}O_6Pd_4S_8Zn$: C, 32.65; H, 1.76; N, 10.88, S, 12.45; Pd, 20.66. Found: C, 32.62; H, 1.69; N, 9.48, S, 11.24; Pd, 23.40%. IR (KBr, cm^{-1}): 3400 (broad), 1632 (w), 1551 (vw), 1516 (w), 1419 (s), 1362 (s), 1317 (m-s), 1252 (m), 1232 (m), 1180 (m-s), 1101 (m-s), 1065 (vw), 1049 (vw), 904 (s), 856 (m), 812 (m), 773 (s), 746 (m), 713 (s), 702 (s), 667 (vw), 565 (vw), 525 (w), 335 (ν Pd–Cl, w).

X-ray Crystallography of $[(CN)_2Th_2Pyz]$. Data were collected on a Bruker APEX II CCD diffractometer using graphite-monochromatized Mo-$K\alpha$ radiation at 295 K. The solution and refinement were carried out using the programs SIR97[6] and SHELX97L.[7]

NMR Measurements on the Solid Crystalline $[(CN)_2Th_2Pyz]$. A solid sample of $[(CN)_2Th_2Pyz]$ was packed into 4 mm zirconia rotors and sealed with Kel-F caps. Solid state ^{13}C CP-MAS NMR spectra were performed at 100.47 MHz on a Bruker AVANCE II 400 spectrometer operating at a static field of 9.4 T and equipped with a 4 mm MAS probe. The spinning speed was 10 kHz. The $\pi/2$ pulse width was 3.5 μs, the relaxation time was 5 s; 18000 scans were acquired. The cross-polarization was made applying the variables spin-lock sequence RAMP-CP-MAS. The contact time τ for the cross-polarization was 2 ms. Spectra were acquired using 1024 data points in the time domain, zero filled and Fourier transformed. Experiments, carried out in the cross-polarization mode with a simultaneous phase inversion (CP-SPI), allowed the different type of carbons to be selectively observed. The contact time τ for the cross-polarization was 2 ms, whereas the length of the pulse used for the phase inversion was 70 μs.

NMR Solution Measurements of $[(CN)_2Th_2Pyz]$ and $[(CN)_2Th_2Pyz(PdCl_2)_2]$. NMR solution measurements of $[(CN)_2Th_2Pyz]$ were made in 700 μL of either DMSO-d_6 or DMF-d_7, and those of $[(CN)_2Th_2Pyz(PdCl_2)_2$ were taken in DMF-d_7 (700 μL). The ^1H and ^{13}C NMR experiments were performed at 27 °C on a Bruker AVANCE AQS 600 spectrometer operating at the 600.13 and 150.95 MHz, respectively, and equipped with a Bruker multinuclear, z gradient probehead.

^{13}C experiments were performed for $[(CN)_2Th_2Pyz]$ using a relaxation delay of 10 s and a GARP sequence to perform proton decoupling. ^1H and ^{13}C assignments were obtained using $^1H-^{13}C$ HSQC and $^1H-^{13}C$ HMBC experiments with a z gradient coherence selection. All 2D experiments were carried out using 1024 data points in the f2 dimension and 512 data points in the f1 dimension; the recycle delay was 1 s. The HSQC experiment was performed using a coupling constant of 150 Hz whereas the delay for the evolution of long-range couplings in the $^1H-^{13}C$ HMBC experiment was 80 ms. ^1H and ^{13}C chemical shifts are reported in parts per million (ppm) and are referred to the residual proton (2.5 ppm) and the residual CH carbon (40.40 ppm) of DMSO-d_6, respectively, or to the residual singlet proton (8.03 ppm) and to the CO (162.5 ppm) of DMF-d_7, respectively.

^1H and ^{13}C assignments were obtained for the bis-palladate $[(CN)_2Th_2Pyz(PdCl_2)_2]$ by means of 2D experiments, namely, $^1H-^1H$ COSY and $^1H-^{13}C$ HSQC. The experiments were carried out using 1024 data points in the f2 dimension and 512 data points in the f1 dimension; the recycle delay was 1 s. HSQC experiments were performed using a coupling constant of 150 Hz. ^1H and ^{13}C chemical shifts are reported in ppm (see below) and are referred to the residual singlet proton and the CO of DMF-d_7, as indicated above. Different samples of the bis-palladate compound gave usually poor response for ^1H and ^{13}C spectra, often disturbed by the presence of little amounts of unknown contaminants. Nevertheless, these measurements allowed to identify proton peak resonance positions and related ^{13}C spectral data of the thienyl rings (see Table 1).

EXAFS Data Collection and Analysis of $[(CN)_2Th_2Pyz(PdCl_2)_2]$. XAS (X-ray Absorption Structure) spectra of solid $[(CN)_2Th_2Pyz(PdCl_2)_2]$ were collected in transmission mode at the ELETTRA Synchrotron (Trieste, Italy) on the beamline 11.1. Solid $[(CN)_2Th_2Pyz(PdCl_2)_2]$ was diluted with boron nitride to give an absorption change over the edge of about one logarithmic unit. The storage ring was operating at 2/2.4 GeV with an optimal storage beam current between 300 and 130 mA. Measurements were carried out at the Pd K-edge, and the incident beam was monochromatized with a Si(111) double crystal. To obtain good signal-to-noise statistic, 5 spectra were recorded and averaged. A Pd foil internal energy calibration was measured simultaneously with each spectrum. The energy was defined by assigning the first inflection point of the Pd foil spectrum to 24350 eV.

EXAFS data analysis was performed using a the GNXAS program which has proven to give reliable structural information also in the high energy domain.[8,9] The GNXAS method accounts for multiple scattering (MS) paths by including the configurational average of all MS signals to allow fitting of correlated distances and bond length variances described by Debye–Waller factors. Because of the short-range sensitivity of the EXAFS technique, only the first coordination shell up to 3.5 Å has been taken into account in the analysis. It comprises two chlorine atoms, one nitrogen, and one sulfur atom. Each theoretical signal has been modeled with a gamma-like function which depends on four parameters, namely, the coordination number N, the average distance R, the distance variance σ^2, and the skewness β. β is related to the third cumulant C_3 of the distance distribution through the relation $C_3 = \sigma^3/\beta$, and R is its first moment of the distance distribution. Additional nonstructural parameters were minimized, namely E_0 (core ionization threshold energy) and S_0^2. Least-squares fits of the EXAFS raw experimental data have been performed by minimizing a residual function (see ref 7). Phase shifts were calculated using muffin-tin potentials and advanced models for the exchange-correlation self-energy (Hedin–Lundqvist). The muffin-tin radii were chosen according to the Norman criterion with 10% of overlapping.

Theoretical Calculations. DFT and TDDFT calculations were performed to provide both gas phase structures and absorption spectra of the two compounds, $[(CN)_2Th_2Pyz]$ and $[(CN)_2Th_2Pyz(PdCl_2)_2]$. The calculations were done with Gaussian03.[10] For the energy calculations and geometric optimizations, the DFT method was used with the B3LYP functional[11] using the 6-311+G(d)[12] basis on the first and second row atoms and the LANL ECP with a TZ basis on the Pd atom.[13] Excited state calculations were performed by means of the TDDFT method[14] using the same functional and the same basis set.

Other Physical Measurements. IR spectra were recorded on a Varian 660-IR FT-IR Spectrometer in the range 4000–250 cm^{-1} (KBr pellets). UV–visible solution spectra were recorded with a Varian Cary 5E spectrometer. Thermogravimetric analyses (TGA) were obtained on a Stanton Redcroft model STA-781 analyzer under a N_2 atmosphere (0.5 L/min). Elemental analyses for C, H, N, and S were provided by the "Servizio di Microanalisi" at the Dipartimento di Chimica, Università "La Sapienza" (Rome) on an EA 1110 CHNS-O instrument. The ICP-PLASMA Pd analyses were performed on a Varian Vista MPX CCD simultaneous ICP-OES. X-ray powder diffraction patterns were obtained on a Philips PW 1710 diffractometer by using a Cu$K\alpha$ (Ni-filtered) radiation.

■ RESULTS AND DISCUSSION

$[(CN)_2Th_2Pyz]$. *X-ray Crystal Structure.* Crystal data and details associated with structure refinements of the dithienyl compound are given in Supporting Information, Table S1. Selected bond distances and angles are summarized in Supporting Information, Table S2. An ORTEP drawing of $[(CN)_2Th_2Pyz]$ is shown in Figure 2. The molecule has a crystallographically imposed m symmetry, with atoms of the dicyanopyrazine ring and the S1/C7–C10 thienyl ring lying on the mirror plane. The thienyl ring containing the S2 atom is orthogonal to the S1/C7–C10 thienyl ring and the rest of the molecule, resulting in the S2 and C12 atoms being alternatively disordered above and below the mirror plane with site occupancy factors of 0.5. The bond distances and angles are as expected and deserve no further comment. The molecular conformation is stabilized by a C–H$\cdots\pi$ hydrogen bond involving the H8 hydrogen atom and the centroid (Cg) of the S2/C11/C13/C13^i/C12^i thienyl ring [symmetry code: (i) = *x*, 0.5−*y*, *z*]: C8−H8, 0.93 Å; H8···Cg, 2.79 Å; C8···Cg, 3.576(3) Å; C8−H8···Cg, 143°] The crystal structure is enforced only by van der Waals interactions. A comparison of the structural data of [$(CN)_2Th_2Pyz$] with those of similar species sharing the presence of two vicinal rings was believed interesting and is shortly discussed in the Supporting Information.

Solid State and Solution NMR Spectra. ^1H and ^{13}C NMR experiments were conducted on [$(CN)_2Th_2Pyz$] in an attempt to make appropriate assignments of the spectral data for the two thienyl rings as a result of their positioning within the molecule in the solid state and in solutions of dimethylformamide (DMF) and dimethyl sulfoxide (DMSO). The NMR spectra in solution are presented first since they show an optimal resolution in terms of peak resonance response. In addition, they provide some help in the interpretation of the solid state spectra, which, as shown later in the manuscript, are more poorly resolved.

^1H and ^{13}C NMR spectra of [$(CN)_2Th_2Pyz$] in DMF-d_7 and ^{13}C spectra of the solid are shown in Figure 3. The spectra measured in DMSO-d_6, which show minimal differences from those taken in DMF-d_7, are given in Supporting Information, Figure S3. All data are summarized in Table 1. For the sake of clarity, assignments of the ^1H and ^{13}C resonances are made using the labeling shown in Figure 2. It is important to note that the CH aromatic protons in DMF-d_7 (in DMSO-d_6 as well) show the same chemical shift, suggesting an equivalence of the two thienyl rings in the molecule. Interestingly, instead, the ^{13}C spectra (see Figure 3B and Supporting Information, Figure S3; Table 4), show an evident nonequivalence of all the CH aromatic signals; in fact, the spectra show two distinct resonances for the couples CH-8 and CH-12′, CH-9 and CH-13′ and for CH-10 and CH-13, whereas all the quaternary carbons, that is, C1 and C2, C3 and C4, C5 and C6, are equivalent. These results indicate that the two thienyl rings statistically occupy, relative to one another, two different positions. From these data it appears, then, that the ^{13}C NMR response is more sensitive to the different positioning of the thienyl rings than that of the protons residing on the same rings. These findings await further support from NMR experiments on molecules carrying similar dithienylpyrazino fragments.

A ^{13}C CP-MAS spectrum of the solid [$(CN)_2Th_2Pyz$] was also examined (Figure 3C). As might be expected, the spectrum is more poorly resolved than the ^{13}C spectra in solution. However, it can be noted that the solution spectrum shows two distinct resonances at 149.19 ppm and 147.87 ppm due to the C1 and C2 carbons belonging to the pyrazine ring. This means that the effect of perturbation due to the orthogonal orientation of the thienyl rings somewhat permeates the pyrazine ring. On the other hand, a distinct response is not seen for the couples CH-8/CH-12′, CH-9/CH-13′ and for CH-10/CH-13, probably because of poor resolution.

To assign the overlapped spectral region between 110 ppm and 140 ppm, the CP-SPI pulse sequence was applied. Using this sequence, a full spectral editing of the CP-MAS spectrum could be obtained. As can be seen in the spectrum of Figure 3D, the methine carbons' resonances are significantly reduced, whereas the resonances due to quaternary atoms are intense and positive. The resonance centered at 138.2 ppm is due to the C7 and C11 quaternary carbons whereas the resonance at 125.1 ppm is due to C-3 and C-4. The resonance at 134.0 ppm is due to C13 and C10, while the resonance at 131.9 ppm is due to C8 and C12′ and C9 and C13; resonances for the C5 and C6 carbons are located at 112.0 ppm. As expected by the CP-SPI sequence, the intensity of these CH resonances is extremely reduced with respect to the intensity of the quaternary carbons. In summary, the NMR data provide useful information concerning the effect of the different orientation of the thienyl rings not only in the solid but also in solution. In addition, the data indicate that the same effect is extended to include the C1 and C2 pyrazine carbon atoms adjacent to the thienyl rings.

DFT and TDDFT Calculations. Support for nonequivalence of the two thienyl rings observed by NMR in the solid, and

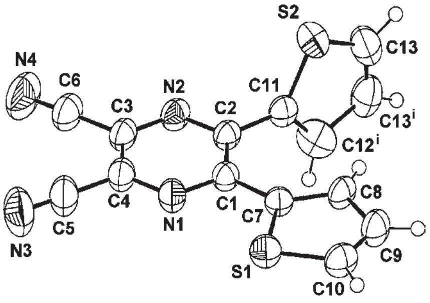

Figure 2. ORTEP view (50% probability ellipsoids) of [$(CN)_2Th_2Pyz$]. Only one component of the disordered thienyl ring containing S2 is shown [symmetry code: (i) *x*, 1/2−*y*, *z*].

Table 1. ^1H and ^{13}C NMR Assignments of [$(CN)_2Th_2Pyz$] in DMF-d_7 and DMSO-d_6 at 300 K[a]

		[$(CN)_2Th_2Pyz$] in DMF-d_7				[$(CN)_2Th_2Pyz$] in DMSO-d_6				solid state
	type	^1H	m	*J* (Hz)	^{13}C	^1H	m	*J* (Hz)	^{13}C	^{13}C
1, 2	C				148.40				148.31	147.87 149.19
3, 4	C				129.29				129.53	125.1
5, 6	C				114.41				114.83	112.0
7, 11	C				138.30				138.20	138.2
8, 12′	CH	7.664	dd	3.8; 1.2	131.93, 132.14	7.549	dd	3.8; 1.0	132.20, 132.38	131.0
9, 13′	CH	7.246	dd	3.8; 5.0	128.94 128.98	7.185	dd	3.8; 5.0	129.49, 129.50	131.0
10, 13	CH	8.067	dd	5.0, 1.2	133.52, 133.69	7.988	dd	5.0, 1.0	134.13, 134.33	134.0

[a] The ^{13}C assignments of [$(CN)_2Th_2Pyz$] in the solid state are also reported in the last column.

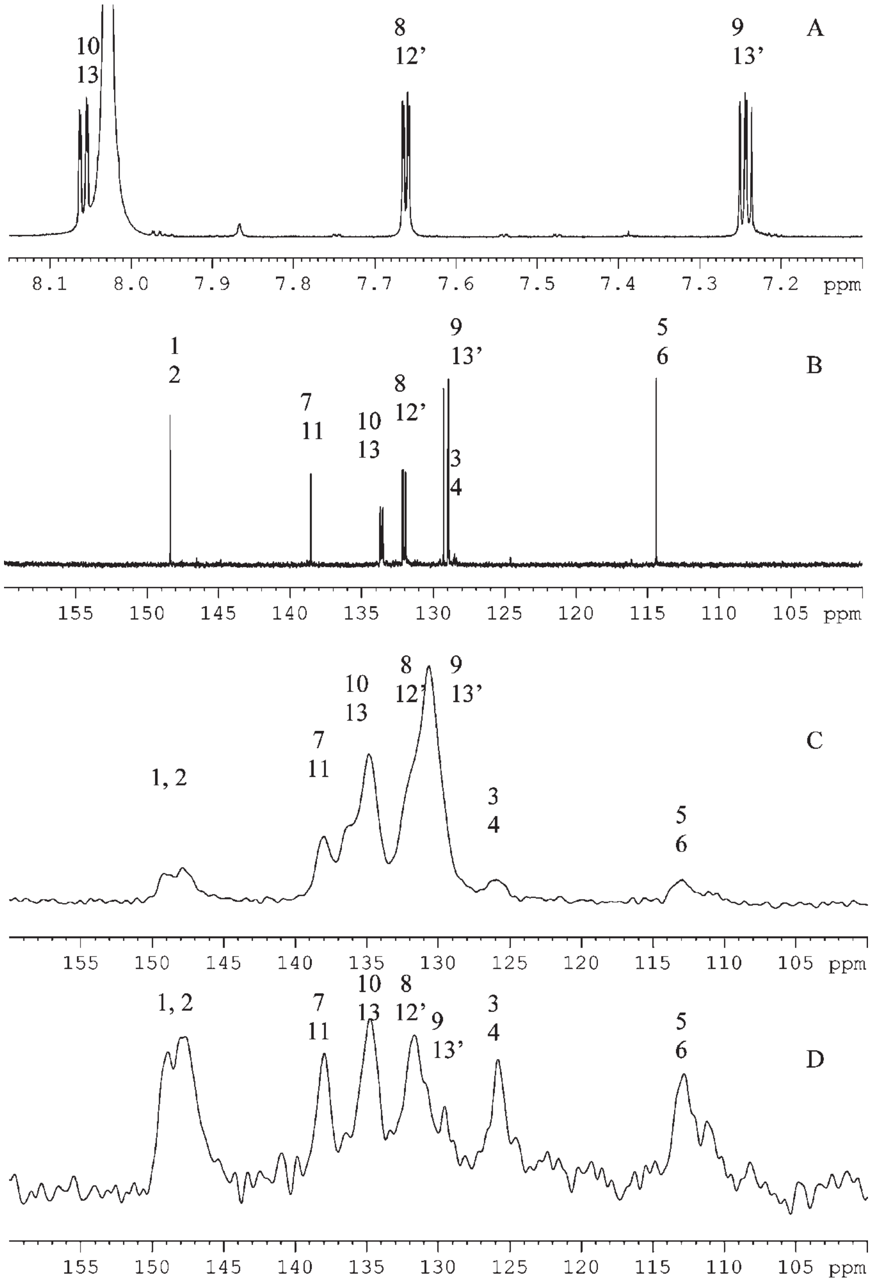

Figure 3. ^{1}H (A) and ^{13}C (B) NMR Spectra of [(CN)$_2$Th$_2$Pyz] in DMF-d_7 at 300 K. ^{13}C CP-MAS Spectrum (C) and ^{13}C CP-SPI Spectrum (D) of [(CN)$_2$Th$_2$Pyz] in the Solid State.

apparently persisting in solution, comes from the DFT/TDDFT calculations, which were directed also to the interpretation of the UV−visible spectrum of the precursor. The gas phase optimized structure of [(CN)$_2$Th$_2$Pyz] is reported in Figure 4. The main difference with the structure in Figure 2 is that the two thienyl rings are not perpendicular to each other. Both are noncoplanar with the pyrazine ring and, noteworthy, the two thienyl rings show the S atoms oriented on the same side. The alternative possibility of having the S atoms both pointing inward has been found to have a higher energy by 1.6 kcal. As to the presently proposed structure, the molecular arrangement is such that the C11−C1−C2−C7 dihedral angle (same labeling of Figure 2) is 19 degrees, while the C6−C3−C4−C5 angle is 9 degrees. These findings fit fairly well with the structure suggested by the NMR spectral data, specifically indicating that the two thienyl rings are not equivalent. The calculated structure, however, does not fit with the X-ray crystal structure. A geometry optimization carried out with GAMESS[15] and a dispersion-corrected density functional (D-B3LYP)[16] produced a structure showing a perpendicular arrangement of the thienyl rings with the ···C−H bond of one thienyl ring pointing toward the π system of the other. Even this structure, however, turned out to have an energy higher by about 1 kcal.

Calculations were extended to interpret the UV−visible spectrum of the precursor which shows intense absorptions in DMF and DMSO solutions at about 310−320 and 380−385 nm (data in Table 2). Figure 5 shows the experimental spectrum in

DMF solution (black line) together with the stick spectrum from TDDFT calculations. The simulated absorption spectrum shows four strong absorption lines at 403.50 nm (3.07 eV; f = 0.19), 397.40 nm (3.12 eV; f = 0.14), 315.10 nm (3.93 eV; f = 0.20) and 249.23 nm (4.97 eV; f = 0.14) with f being the oscillator strength. The first two lines, 403.50 and 397.40 nm, are responsible for the strong band observed experimentally at 380−385 nm, the third line at 315.10 nm for the band seen at 310−320 nm. The fourth line falls outside the detection range of the experiments. The agreement between the experimental spectral data and calculated values is quite satisfactory. The first two lines are due to electronic transitions between the highest occupied molecular orbital (HOMO) and the lowest unoccupied molecular orbital (LUMO) and LUMO+1 ones. The three orbitals, shown in Supporting Information, Figure S4, are loosely classifiable as π and π^* orbitals, although the molecule is non planar. The HOMO → LUMO transition resembles a $\pi \rightarrow \pi^*$ transition, but it brings considerable electronic density from the thienyl rings onto the pyrazine one. This effect is even more pronounced for the second absorption line at 397 nm which involves the transition HOMO → LUMO+1. The second absorption band measured at 310−320 nm (calcd 315.10 nm) is instead due to a series of complicated electronic transitions from the HOMO-1, HOMO-2, and HOMO-3 orbitals into the LUMO and LUMO+1 ones. Supporting Information, Figure S4 shows that the HOMO-2 and HOMO-3 orbitals are completely localized on the thienyl rings .

$[(CN)_2Th_2Pyz(PdCl_2)_2]\cdot H_2O$. The structure of the air stable $[(CN)_2Th_2Pyz(PdCl_2)_2]\cdot H_2O$ complex was examined by ^1H and ^{13}C NMR and UV−visible spectra. EXAFS on the solid material and also DFT and TDDFT calculations were carried out to obtain a more complete structural and UV−visible spectral characterization of the material.

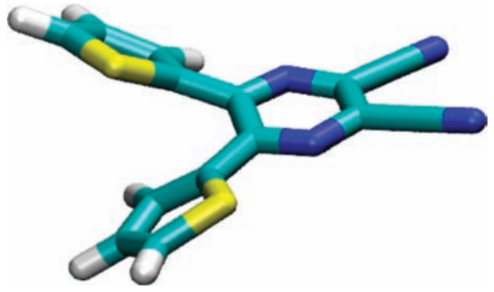

Figure 4. Optimized gas phase structure of $[(CN)_2Th_2Pyz]$.

NMR Spectral Data. ^1H and ^{13}C NMR spectra on the bispalladate derivative were obtained in DMF-d_7. The presence of a unique triad of proton resonance peaks (left side of Table 3) indicates that the two thienyl rings do not differ from each other in terms of their proton resonance response. Peak resonance positions are different from those of the unmetalated species in the same solvent (Table 1), suggesting that the thienyl groups are both directly involved in Pd^{II} coordination. The data available, however, do not provide adequate information about the relative orientation of the vicinal thienyl rings in the complex and their involvement in coordination around the Pd^{II} centers. More satisfactory information is given by EXAFS measurements and DFT calculations, as discussed below.

EXAFS Results. A quantitative determination of the coordination geometry of Pd^{II} in $[(CN)_2Th_2Pyz(PdCl_2)_2]$ was obtained

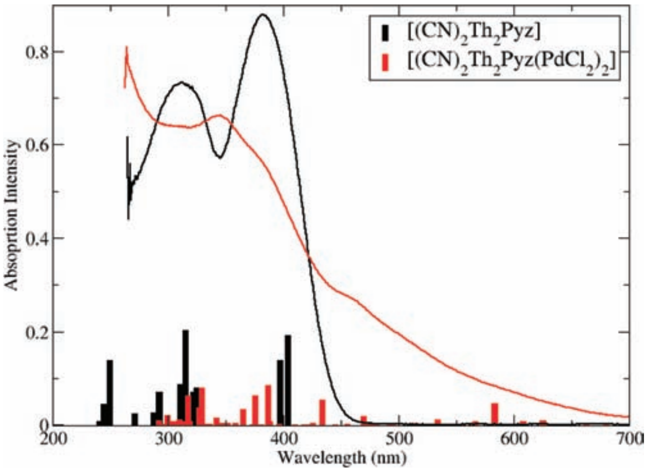

Figure 5. UV−visible solution spectra in DMF of $[(CN)_2Th_2Pyz]$ (black line; c = 5.9 × 10^{-5} M)) and its bis-palladate derivative $[(CN)_2Th_2Pyz(PdCl_2)_2]$ (red line; c = 4.0 × 10^{-5} M). Sticks are from theoretical calculations.

Table 2. UV-visible Spectral Data of $[(CN)_2Th_2Pyz]$ and $[(CN)_2Th_2Pyz(PdCl_2)_2]\cdot H_2O$ in DMF and DMSO

compound	solvent	λ, nm (log ε)		
$[(CN)_2Th_2Pyz]$	DMF	311 (4.08)	383 (4.16)	
	DMSO	319 (4.07)	384 (4.21)	
$[(CN)_2Th_2Pyz(PdCl_2)_2]\cdot H_2O$	DMF	346 (4.26)	371(sh) (4.20)	469(sh) (3.80)
	DMSO	329 (4.37)	375(sh) (4.20)	467(sh) (3.80)

Table 3. ^1H and ^{13}C NMR Assignments of $[(CN)_2Th_2Pyz(PdCl_2)_2]\cdot H_2O$ in DMF-d_7 and ^1H NMR Data of the Complexes $[Th_8TPyzPzMg(H_2O)]$ and $[(PdCl_2)_4Th_8TPyzPzMg(H_2O)]$ in DMSO-d_6 at 300 K

	$[(CN)_2Th_2Pyz(PdCl_2)_2]\cdot H_2O$				$[Th_8TPyzPzMg(H_2O)]$			$[(PdCl_2)_4Th_8TPyzPzMg(H_2O)]$		
a	^1H (ppm)	m	J(Hz)	^{13}C (ppm)	^1H (ppm)	m	J(Hz)	^1H (ppm)	m	J(Hz)
5	8.12	dd	5.0, 1.2	132.0	8.037	d	5.1	8.050	d	5.0
4	7.39	dd	5.0, 3.6	128.0	7.343	dd	5.1, 3.6	7.351	dd	5.0; 3.0
3	8.0	h^b		131.0	7.646	d	3.6	7.670	bd	3.0

[a] See Chart 1, panel A. [b] h = hidden: the assignment was obtained by means of the ^1H−^1H COSY experiment.

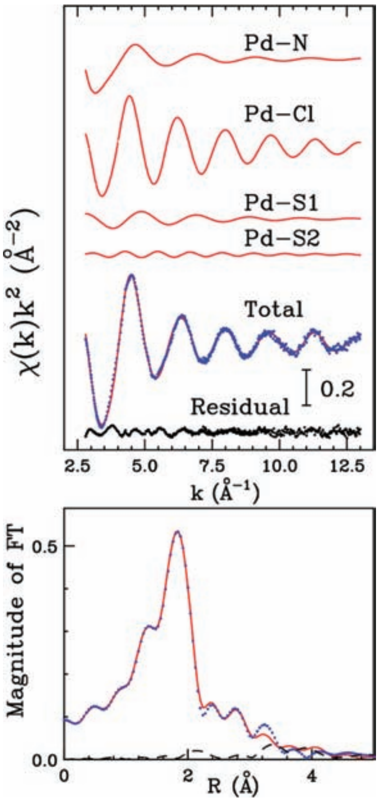

Figure 6. Analysis of the Pd K-edge EXAFS spectrum of solid $[(CN)_2Th_2Pyz(PdCl_2)_2]$. Upper panel: theoretical Pd–N, Pd–Cl, and Pd–S first shell contributions, total theoretical signal (full red line) compared with the experimental spectrum (dotted blue line), and residual curve (full black line). Lower panel: nonphase-shift-corrected Fourier transforms of the experimental data (dotted blue line), of the total theoretical signal (full red line), and of the residual curve (dashed-dotted black line).

Table 4. Palladium(II) First Shell Geometrical Parameters Obtained by EXAFS on $[(CN)_2Th_2Pyz(PdCl_2)_2]$[a]

	N	R (Å)	σ^2 (Å^2)	β	R (Å)
Pd–N	1	2.03(3)	0.020(4)	0.9(3)	2.12–2.14
Pd–Cl	2	2.36(3)	0.011(4)	0.9(3)	2.28–2.29
Pd–S1	0.5	2.25(4)	0.019(5)	1.1(3)	2.46–3.5
Pd–S2	0.5	3.21(5)	0.025(5)	1.2(3)	

[a] N is the coordination number, R the average distance, σ^2 the distance variance, and β is the skewness. The last column reports the bond distances obtained by DFT calculations.

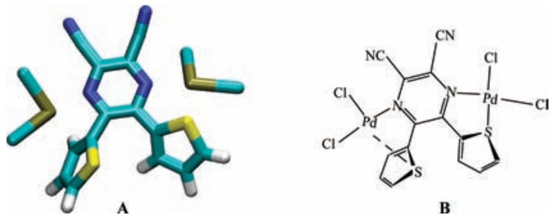

Figure 7. Calculated optimized structure (A) and schematic representation (B) for the bis-palladate compound $[(CN)_2Th_2Pyz(PdCl_2)_2]$.

by assuming the first coordination sphere of each Pd^{II} center in the compound as being composed of two Cl atoms, one N atom of the pyrazine ring, and possibly the S atom of one thienyl ring. Fitting procedures were applied to the whole set of structural and nonstructural parameters to improve, as far as possible, the agreement between the calculated signals and the experimental EXAFS spectrum. In particular, we optimized four structural parameters for each single shell contribution, and least-squares fits were performed in the range k = 2.5–12.8 Å^{-1}. The best-fit analysis is shown in the upper panel of Figure 6. The first four curves from the top are the Pd–N, Pd–Cl, and Pd–S first shell two-body contributions, and the remainder of the figure shows the total theoretical signal compared with the experimental spectrum, and the resulting residual. Overall, the fitted EXAFS spectrum matches the experimental data well enough, and the dominant contribution to the total EXAFS signals is given by the Pd–Cl first shell signal, because of the multiplicity of two, and to the Pd–N signal. Moreover, one of the S atoms also provides a detectable contribution well above the experimental noise of the spectrum. The FT moduli of the experimental spectra extracted with a three segmented cubic spline are shown in the lower panel of Figure 6. The FTs have been calculated in the interval k = 2.5–12.5 Å^{-1} with no phase-shift correction applied. The agreement between the theoretical and the experimental curves is quite good, reinforcing the validity of the following structural results. Elaboration of EXAFS experimental data provide evidence of the occurrence of two different Pd^{II} coordination sites. In one of them, Pd^{II} first shell was fitted with one Pd–N contribution with a distance of 2.03 ± 0.03 Å, two Pd–Cl contributions with a distance of 2.36 ± 0.03 Å and one Pd–S contribution with a distance of 2.25 ± 0.04 Å (Table 4). The presence of a short Pd–S bond distance hinders a comparable approach for the second S atom to the Pd^{II} center, the coordination site of which sees the S atom at a much longer distance (3.21 ± 0.05 Å), in an overall asymmetric arrangement of the entire molecular framework. The relatively low intensity of both the Pd–S signals is probably due to the coexistence of two different Pd^{II} coordination environments.

DFT and TDDFT Calculations. Data from DFT studies of $[(CN)_2Th_2Pyz(PdCl_2)_2]$ concerning the Pd–N, Pd–Cl, and Pd–S bond distances are reported in Table 4 (last column). As can be seen, the Pd–N and Pd–Cl bond distances of the optimized structure are in good agreement with those obtained from elaboration of the EXAFS experiments. Two Pd–S bond distances are obtained from calculations, both sufficiently close to those obtained from the EXAFS. This generates the structurally distorted arrangement shown in Figure 7, where it can be seen that the two thienyl rings are oriented with the S atoms on the same side, displaying a quite different approach to the two Pd^{II} centers. Formation of this nonsymmetrical arrangement might be explained by assuming that after the binding of the first $PdCl_2$ unit at a distance of 2.25(4) Å (Table 4), the second unit binds preferably the N atom, but the S atom of the second thienyl ring is at a longer distance.

Figure 5 shows the experimental absorption spectrum for this bis-palladate compound (red line). Sticks from TDDFT calculations are also presented. Theoretically, it has been found that the complex molecule has a much greater density of states than its precursor $[(CN)_2Th_2Pyz]$. The absorptions below 450 nm, in a fashion similar to what has been found for the precursor

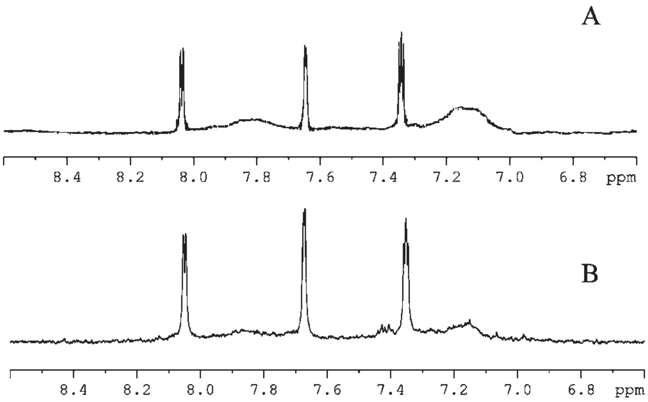

Figure 8. ^{1}H NMR Spectra in DMSO-d_6 at 300 K of [$Th_8TPyzPzMg(H_2O)$] (A) and [$(PdCl_2)_4Th_8TPyzPzMg(H_2O)$] (B).

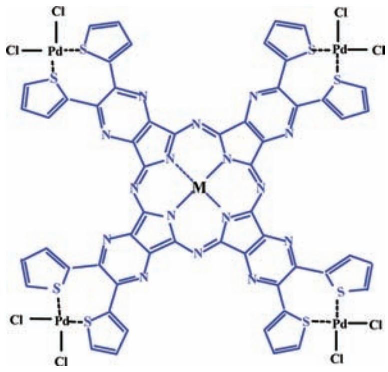

Figure 9. Schematic representation of the pentanuclear macrocycles [$(PdCl_2)_4Th_8TPyzPzM$] (M = $Mg^{II}(H_2O)$, Zn^{II}).

[$(CN)_2Th_2Pyz$], are due to $\pi \rightarrow \pi^*$ absorption processes that bring the electronic density from the thienyl groups to the pyrazine ring (Supporting Information, Figure S4). The stick spectra of the bis-palladate compound is qualitatively in agreement with the experimental one as it remains quite unstructured without showing prominent absorption peaks. It should be noted that, in the case of the bis-palladate, we were able to perform calculations only down to 290 nm, that is, the energy corresponding to the 70th excited state.

The low-energy part of the absorption spectrum above 450 nm is due to transitions from nonbonding orbitals localized on the two $PdCl_2$ units (because of combinations of the p functions of Cl and the d functions of Pd) to the π^* orbitals. Specifically, the sizable absorption band predicted by our calculations to be at 583 nm is due to a mixed excitation process, roughly dominated by a single electron excitation from the d and p orbitals of $PdCl_2$ to the π^* orbitals.

Porphyrazine Macrocycles [$(PdCl_2)_4Th_8TPyzPzM$] (M = $Mg^{II}(H_2O)$, Zn^{II}). *General Properties.* Intensively colored dark green heteropentametallic macrocycles having the formula [$(PdCl_2)_4Th_8TPyzPzM$] (M = $Mg^{II}(H_2O)$, Zn^{II}) were obtained from the parent mononuclear species [$Th_8TPyzPzM$][3] (Figure 1) by reaction with $PdCl_2$ under the specified conditions (see Experimental Section). All attempts to generate [$(PdCl_2)_8Th_8TPyzPzM$] as an additional product by using excess $PdCl_2$ were unsuccessful, and it is reasonably assumed that the arrangement of eight $PdCl_2$ units between vicinal dipyridinopyrazine moieties in the macrocycle would lead to excessive crowding and high steric hindrance.

The two complexes usually contain clathrated water, the amount of which is variable from batch to batch for the single species, with a negligible influence on the general physicochemical behavior of the compounds, and it is therefore taken into account only for quantitative aspects. The two macrocycles are completely insoluble in water and in nondonor organic solvents (CH_2Cl_2, $CHCl_3$, THF, C_6H_5CN) and are only slightly soluble in the low-donor solvents pyridine, DMSO, and DMF, in which their UV−visible behavior and NMR spectral response have been examined (see below).

It must be noted that the observed formation of octathienyl macrocycles bearing externally coordinated four $PdCl_2$ units implies the binding of one $PdCl_2$ unit for each single di(2-thienyl)pyrazino fragment, a situation definitely distinct from that found for the metalated precursor, in which the $PdCl_2$: fragment ratio is 2:1. This evidently determines a different involvement of the exocyclic thienyl rings in the binding to Pd^{II}. The $PdCl_2$ units appear to be consistently ligated to the di(2-thienyl)pyrazino fragments, more strongly than in the parallel series of homo-[2b] and heteropentametallic[2g] octapyridinated macrocycles. In fact, under comparable experimental conditions in which for these latter compounds $PdCl_2$ units are released (contact for 1−2 h at room temperature with pyridine or diluted NH_3), the present octathienyl compounds remain unchanged.

NMR Spectral Data. The ^{1}H NMR spectral data in DMSO-d_6 of the Mg^{II} complex [$Th_8TPyzPzMg^{II}(H_2O)$] and its corresponding tetrapalladated species [$(PdCl_2)_4Th_8TPyzPzMg^{II}(H_2O)$] are shown in Figure 8. The spectra show three well resolved proton resonance peaks (ppm) assigned to the thienyl rings of both the mono- (Figure 8A) and the pentametallic species (Figure 8B). Interestingly, the data in Table 3 indicate that the peaks of the latter species are shifted slightly to lower fields with respect to those of the mononuclear species, and the spectrum reveals that no residual peaks of the mononuclear compound are present. From these data, it can be reasonably suggested that, in the pentanuclear species, the vicinal thienyl rings present in each one of the four di(2-thienyl)pyrazino fragments are directly involved in the coordination to Pd^{II} ("th-th" coordination) with formation of $S_{2(th)}PdCl_2$ coordination sites (Figure 9), closely recalling the "py-py" coordination established for the related externally tetrapalladated octapiridinated analogues.[2b,g] Formation of short S−Pd bonds, of the type found for one Pd^{II} center in the bispalladate compound (2.25(4) Å) (Table 4), is in keeping with the observed high stability of the palladated macrocycle.

UV−visible Spectral Behavior. UV−visible spectra in pyridine, DMSO, and DMF of the mono- and pentametallic species at concentrations of about 1.0×10^{-5} M (or lower) are stable and typical of clean monomeric species, with a Soret band and relatively more intense sharp Q bands in the regions 390−400 and 670−675 nm, respectively (data in Table 5). At concentrations higher than 1.0×10^{-5} M, with the upper limit of about 5.0×10^{-4} M (saturation), the spectra may indicate the presence of aggregation. Figure 10 shows the spectral features of the pentanuclear Mg^{II} complex in DMF at three different concentrations. Spectrum "a" taken at $c = 5.0 \times 10^{-6}$ M shows uniquely the presence of the complex in its monomeric form, quantitative data of which have been calculated. In spectrum "b" ($c \cong 1.0 \times 10^{-5}$ M) the monomeric form is still prevailing, but in spectrum "c" ($c \cong 5.0 \times 10^{-4}$ M) aggregation is largely present. The tendency to aggregate is similar for the Zn^{II} analogue at comparable concentrations but some tendency of the aggregated species to disappear with time is occasionally seen, depending on the solvent and specific batch preparation.

It is observed that peak positions for the monometallic Mg^{II}-(H_2O) and Zn^{II} species (Table 5) show practically no solvent dependence and no spectral changes are observed as a function of time or the central metal ion. It is noteworthy that the mono- and pentametallic octathienyl compounds maintain both the Soret and Q-band positions bathochromically shifted with respect to what is observed for the corresponding octapyridino analogues (Table 5). This seems to indicate, as earlier suggested,[3] that the thienyl residues behave as stronger electron-withdrawing groups than the pyridine rings in the related macrocycles. An interesting aspect of the spectra is that the Soret and Q bands remain unshifted upon exocyclic coordination of the $PdCl_2$ units. This is different from what has been seen for the parallel series of octapyridino analogues,[2b,g] for which peripheral coordination of $PdCl_2$ units leads to a bathochromic shift of 7−9 nm in DMSO (data reported in Table 5) or the other solvents. To find an adequate explanation, these findings require a knowledge of the precise local geometry at the Pd^{II} coordination sites as well as an understanding of how the pyridyl and thienyl rings are positioned with respect to the central pyrazinoporphyrazine core, a fact which may significantly influence the σ/π electronic contact between the central macrocyclic framework and the peripheral metalated fragments.

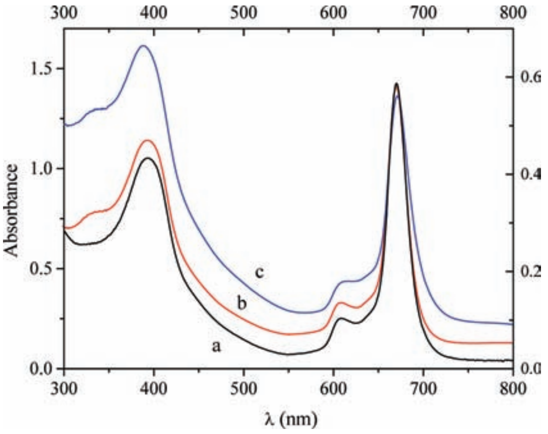

Figure 10. UV−visible spectra of $[(PdCl_2)_4Th_8TPyzPzMg(H_2O)]$ in DMSO: (a) $c = 5.0 \times 10^{-6}$ M (quantitative spectrum, right Y scale); (b) c = ca. 1.5×10^{-5} M; (c) c = ca. 5.0×10^{-4} M.

■ CONCLUSIONS

It has been established by single crystal X-ray work that the compound 2,3-dicyano-5,6-di(2-thienyl)-1,4-pyrazine, $[(CN)_2Th_2Pyz]$ contains the two vicinal thienyl groups orthogonal to each other in the solid. ^1H and ^{13}C NMR studies confirm the non equivalence of the same thienyl rings in the solid state and that some type of non equivalence is maintained in solution. The same compound acts as a precursor for the formation of a bis-palladate derivative $[(CN)_2Th_2Pyz(PdCl_2)_2]$ by reaction with $PdCl_2$. As established by EXAFS studies and supported by DFT theoretical calculations, two different coordination sites occur in the complex, in which the two $PdCl_2$ units are ligated to a pyrazine N atom and to a S atom, generating different local environments for the Pd^{II} centers and an overall asymmetric structure. This asymmetric arrangement might be the source for the observed amorphous character of the solid compound. This behavior is different from what has been observed for its monopalladated bispyridine analogue $[(CN)_2Py_2PyzPdCl_2]$, a crystalline solid, where Pd^{II} is involved in a square planar $N_{2(pyr)}PdCl_2$ coordination site. DFT and TDDFT calculations adequately explain the UV−visible spectral behavior of both $[(CN)_2Th_2Pyz]$ and the complex $[(CN)_2Th_2Pyz(PdCl_2)_2]$. The data presented strongly suggest an equivalent employment of vicinal 2-thienyl rings in the macrocycles $[(PdCl_2)_4Th_8TPyzPzM]$ ($M = Mg^{II}(H_2O), Zn^{II}$) through their sulfur atoms and formation of exocyclic $S_{2(th)}PdCl_2$ coordination sites, a type of binding distinct from that observed for the bispalladate compound $[(CN)_2Th_2Pyz(PdCl_2)_2]\cdot H_2O$.

Table 5. UV-visible Solution Spectra in Pyridine, DMSO, and DMF of the Octathienyl Macrocycles and Related Species

compound	solvent	Soret region λ [nm] (log ε)	Q-band region λ [nm] (log ε)				ref.
$[(PdCl_2)_4Th_8TPyzPzMg(H_2O)]$	py	391 (4.90)			612 (4.37)	672 (5.10)	tw
	DMSO	394 (4.96)			609 (4.35)	670 (5.11)	tw
	DMF	389 (4.90)			609 (4.40)	675 (5.16)	tw
$[(PdCl_2)_4Th_8TPyzPzZn]$	py	393 (4.90)			610 (4.40)	673 (5.20)	tw
	DMSO	393 (4.80)			609 (4.40)	673 (5.03)	tw
	DMF	397 (4.70)			609 (4.20)	672 (4.90)	tw
$[Th_8TPyzPzMg(H_2O)]\cdot 5H_2O$	py	387 (4.90)			609 (4.30)	674 (5.04)	3
	DMSO	394 (4.90)			611 (4.50)	672(4.90)	3
	DMF	386 (4.90)			608 (4.30)	672 (5.04)	3
$[Th_8TPyzPzZn]\cdot 4H_2O$	py	393 (5.10)			608 (4.60)	674 (5.40)	3
	DMSO	390 (5.03)			609 (4.41)	672 (5.30)	3
	DMF	395 (5.09)			609 (4.50)	672 (5.40)	3
$[(PdCl_2)_4Py_8TPyzPzMg(H_2O)]$	DMSO	360 (5.19)			603 (4.66)	660 (5.29)	2g
	DMF	368 (5.20)			603 (4.81)	662 (5.40)	2g
$[(PdCl_2)_4Py_8TPyzPzZn]$	DMSO	378 (4.60)			600 (4.18)	664 (4.88)	2g
	DMF	379 (4.66)			603 (4.21)	662 (4.96)	2g
$[Py_8TPyzPzMg(H_2O)]$	py	375 (5.23)		596 (4.65)	631 (sh) (4.64)	658 (5.54)	2c
	DMSO	374 (5.08)	566 (sh) (3.96)	594 (4.36)	629 (sh) (4.55)	653 (5.34)	2f
$[Py_8TPyzPzZn]$	py	378 (4.90)		598 (4.31)	630 (sh) (4.35)	658 (5.18)	2c
	DMSO	372 (5.10)	565 (sh) (4.02)	592 (4.54)	629 (sh) (4.61)	655 (5.36)	2f

Overall, the data presented provide information about the multifaceted mode of coordination of vicinal thienyl rings to a metal center.

■ ASSOCIATED CONTENT

Ⓢ Supporting Information. Scheme S1 with the types of Pd-thienyl bonds. X-ray crystallographic data in CIF format; Figures S1−S2 have details of the X-ray data collection and structure analysis, Table S1 has experimental data, and Table S2 listing of selected bond distances and angles of $[(CN)_2Th_2Pyz]$. A short presentation of data on the structural features of $[(CN)_2Th_2Pyz]$ in comparison with those of related species carrying vicinal thienyl rings. Figure S3 showing ^1H and ^{13}C NMR spectra of $[(CN)_2Th_2Pyz]$ in DMSO-d_6. Figure S4 showing the molecular Kohn−Sham HOMO, LUMO, and LUMO-1 orbitals for the precursor $[(CN)_2Th_2Pyz]$. This material is available free of charge via the Internet at http://pubs.acs.org. Tables containing the optimized geometries of the precursor and the bis-palladate complex in XYZ format are available on request (enrico.bodo@uniroma1.it).

■ AUTHOR INFORMATION

Corresponding Author

*E-mail: mariapia.donzello@uniroma1.it.

■ ACKNOWLEDGMENT

M.P.D. acknowledges financial help from the MIUR (Ministero dell'Università e della Ricerca Scientifica; PRIN 2007XWBRR4) and by the University of Rome La Sapienza. K.K. acknowledges support of the Robert A. Welch Foundation (K.M.K, Grant E-680). G.D.M. thanks the CIRCMSB for an annual grant. E.B. is grateful to CASPUR supercomputing center for the computational support. Thanks to L. Astolfi for assistance with elemental analyses (Pd) on the Varian Vista MPX CCD apparatus.

■ REFERENCES

(1) Cai, X.; Donzello, M. P.; Viola, E.; Rizzoli, C.; Ercolani, C.; Kadish, K. M. *Inorg. Chem.* **2009**, *48*, 7086.

(2) (a) Donzello, M. P.; Ou, Z.; Monacelli, F.; Ricciardi, G.; Rizzoli, C.; Ercolani, C.; Kadish, K. M. *Inorg. Chem.* **2004**, *43*, 8626. (b) Donzello, M. P.; Viola, E.; Xiaohui, C.; Mannina, L.; Rizzoli, C.; Ricciardi, G.; Ercolani, C.; Kadish, K. M.; Rosa, A. *Inorg. Chem.* **2008**, *47*, 3903. (c) Donzello, M. P.; Ou, Z.; Dini, D.; Meneghetti, M.; Ercolani, C.; Kadish, K. M. *Inorg. Chem.* **2004**, *43*, 8637. (d) Viola, E.; Donzello, M. P.; Ciattini, S.; Portatone, G.; Ercolani, C. *Eur. J. Inorg. Chem.* **2009**, 1600. (e) Bergami, C.; Donzello, M. P.; Ercolani, C.; Monacelli, F.; Kadish, K. M.; Rizzoli, C. *Inorg. Chem.* **2005**, *44*, 9852. (f) Bergami, C.; Donzello, M. P.; Monacelli, F.; Ercolani, C.; Kadish, K. M. *Inorg. Chem.* **2005**, *44*, 9862. (g) Donzello, M. P.; Viola, E.; Cai, X.; Mannina, L.; Ercolani, C.; Kadish, K. M. *Inorg. Chem.* **2010**, *49*, 2447.

(3) De Mori, G.; Fu, Z.; Viola, E.; Cai, X.; Ercolani, C.; Donzello, M. P.; Kadish, K. M. *Inorg. Chem.* **2011**, *50*, 8225.

(4) (a) Mørkved, E. H.; Ossleten, H.; Kjøsen, H.; Bjørlo, O. *J. Prakt. Chem.* **2000**, *342*, 83. (b) Mørkved, E. H.; Afseth, N. Kr.; Zimcik, P. *J. Porphyrins Phthalocyanines* **2007**, *11*, 130.

(5) Kharasch, M. S.; Seyler, R. C.; Mayor, F. R. *J. Am. Chem. Soc.* **1938**, *60*, 882.

(6) Altomare, A.; Burla, M. C.; Camalli, M.; Cascarano, G.; Giacovazzo, C.; Guagliardi, A.; Moliterni, A. G. G.; Polidori, G.; Spagna, R. *J. Appl. Crystallogr.* **1999**, *32*, 115.

(7) Sheldrick, G. M. *Acta Crystallogr.* **2008**, *A64*, 112.

(8) Filipponi, A.; Di Cicco, A.; Natoli, C. R. *Phys. Rev. B* **1995**, *52*, 15122.

(9) Filipponi, A.; Di Cicco, A. *Phys. Rev. B.* **1995**, *52*, 15135.

(10) Frisch, M. J.; Trucks, G. W.; Schlegel, H. B.; Scuseria, G. E.; Robb, M. A.; Cheeseman, J. R.; Scalmani, G.; Barone, V.; Mennucci, B.; Petersson, G. A.; Nakatsuji, H.; Caricato, M.; Li, X.; Hratchian, H. P.; Izmaylov, A. F.; Bloino, J.; Zheng, G.; Sonnenberg, J. L.; Hada, M.; Ehara, M.; Toyota, K.; Fukuda, R.; Hasegawa, J.; Ishida, M.; Nakajima, T.; Honda, Y.; Kitao, O.; Nakai, H.; Vreven, T.; Montgomery, J. A., Jr.; Peralta, J. E.; Ogliaro, F.; Bearpark, M.; Heyd, J. J.; Brothers, E.; Kudin, K. N.; Staroverov, V. N.; Kobayashi, R.; Normand, J.; Raghavachari, K.; Rendell, A.; Burant, J. C.; Iyengar, S. S.; Tomasi, J.; Cossi, M.; Rega, N.; Millam, J. M.; Klene, M.; Knox, J. E.; Cross, J. B.; Bakken, V.; Adamo, C.; Jaramillo, J.; Gomperts, R.; Stratmann, R. E.; Yazyev, O.; Austin, A. J.; Cammi, R.; Pomelli, C.; Ochterski, J. W.; Martin, R. L.; Morokuma, K.; Zakrzewski, V. G.; Voth, G. A.; Salvador, P.; Dannenberg, J. J.; Dapprich, S.; Daniels, A. D.; Farkas, Ö.; Foresman, J. B.; Ortiz, J. V.; Cioslowski, J.; Fox, D. J. *Gaussian 09*, Revision A.1; Gaussian, Inc.: Wallingford, CT, 2009.

(11) Becke, A. D. *J. Chem. Phys.* **1993**, *98*, 5648.

(12) McLean, A. D.; Chandler, G. S. *J. Chem. Phys.* **1980**, *72*, 5639.

(13) Hay, P. J.; Wadt, W. R. *J. Chem. Phys.* **1985**, *82*, 299.

(14) Casida, M. E.; Jamorski, C.; Casida, K. C.; Salahub, D. R. *J. Chem. Phys.* **1998**, *108*, 4439.

(15) Schmidt, M. W.; Baldridge, K. K.; Boatz, J. A.; Elbert, S. T.; Gordon, M. S.; Jensen, J. H.; Koseki, S.; Matsunaga, N.; Nguyen, K. A.; Su, S.; Windus, T. L.; Dupuis, M.; Montgomery, J. A. *J. Comput. Chem.* **1993**, *14*, 1347.

(16) Grimme, S. *J. Comput. Chem.* **2006**, *27*, 1787.